Langmuir

Article

pubs.acs.org/Langmuir

Shear History Independence in Colloidal Aggregation

William R. Heinson, Christopher M. Sorensen, and Amitabha Chakrabarti*

Department of Physics, Kansas State University, Manhattan, Kansas 66506, United States

ABSTRACT: Stimulated by experiments, we have carried out detailed simulations of aggregation in the presence of shear in a model colloidal system with a short-range attractive potential. For weak shear rates, we find that the shear enhanced the aggregation and that the long-time state of the system is independent of the shear history. For strong shear rates, precipitous fragmentation occurred after the shear was turned on and, after an induction period, the aggregation quickly rebounded in a stochastic manner similar to classical nucleation phenomena. However, the long-time state of the system is, once again, independent of the shear history. Thus, for both weak and strong shear cases, the shear rate acts as a state variable of the aggregating system. Shear rates employed in the simulations can be attained in laboratory experiments, as confirmed by computing the dimensionless Péclet numbers.

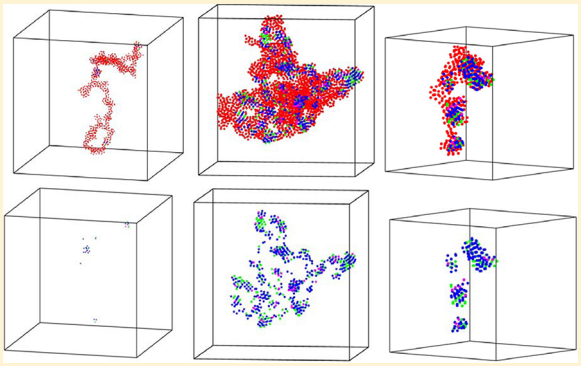

1. INTRODUCTION

Aggregation is a fundamental growth process for all dispersions of particulate matter. We view aggregation as encompassing any process that brings particles together to form a connected body, from irreversible fractal aggregate formation to the reversible precipitation of molecules from solution to form crystalline solids. Thus, the aggregation process is fundamentally important for colloids and aerosols and even solutions and, hence, plays an important role in many areas of science and technology.[1] The aggregation of particles depends upon their relative motion and interaction potential. Brownian motion, which is driven by thermal energy, is always present to cause aggregation. Other important mechanisms to create relative motion include shear, turbulent shear, and gravitational settling. The interaction potential depends upon the nature of the particles and the suspending medium.

Our focus in this paper is on the influence of shear on aggregation. Many experimental and theoretical studies have been carried out to investigate the effect of shear flow on the kinetics of aggregation,[2−16] the resulting size distributions, and structures of particle aggregates. To summarize these findings, previous shear experiments have seen either fragmentation because of shear, restructuring as indicated by fractal dimensions larger than the diffusion-limited cluster aggregation (DLCA) value of $D = 1.8$ or experienced both fragmentation and restructuring. Often the shear fragmentation was eventually balanced by the aggregation, and a steady state was reached. The shear aggregation in these studies was dominant over Brownian aggregation.

The numerical simulations presented in this paper have been stimulated by two experiments in our laboratory, which strongly suggest that there is a great bounty of new phenomena that have neither been explored nor possibly even discovered when a dispersion of colloidal particles undergoes aggregation under the influence of shear.[17,18] In laboratory experiments in ref 17, aqueous solutions of gelatin of mass $M_w = 1.2 \times 10^5$ Da were prepared at 3.0% by weight using deionized water. Once dissolved, the solutions were held at 45 °C for 1 h to dissociate the gelatin molecular agglomerates. These hot solutions were then quenched to 28 °C, which is below the gel temperature of ca. 30 °C. Viscosities were measured as a function of time after quench. Shear rates of between 3.75 and 750 s^{-1} were applied at different times after quench. Regardless of shear start time, the measured viscosities quickly changed to the values that they would have had at that time had the shear been present from the beginning. This implies shear rate history independence for aggregation and gelation of gelatin solutions under the influence of shear.[17] The experimental study in ref 18 involved shearing an aqueous suspension of 20 nm polystyrene latex microspheres. $MgCl_2$ was added to induce aggregation, and the particles interacted via the primary minimum of the DLVO potential. The sample was sheared once for approximately 33 s at different times, typically 1, 5, or 15 min, after the onset of aggregation, with shear rates in the range of 0.13−3.56 s^{-1}. Experiments show that for modest shears, as indicated by the Péclet number being in the range of unity (unlike any previous work), shear can enhance the aggregation and gelation rate but the aggregates formed under shear can be either fractal or hybrid mixed fractal structures.[18]

Our results presented here provide the first theoretical support to these scattered clues seen in experiments on complex systems. Simulation results are clean and deal with a simple aggregating system in the presence of shear with a well-studied short-range attractive potential. Shear rates employed in

Received: May 16, 2012
Revised: June 29, 2012
Published: July 15, 2012

the simulations can be attained in laboratory experiments, as confirmed by computing the dimensionless Péclet numbers for the simulation studies. For weak shear rates (characterized by Péclet numbers less than unity), we find that the shear enhanced the aggregation and that the long-time state of the system is independent of the shear history. For strong shear rates, precipitous fragmentation occurred after the shear was turned on and, after an induction period, in which numerous runs were shown to be stochastic, the aggregation quickly rebounded in a manner similar to classical nucleation phenomena. However, the long-time state of the system is, once again, independent of the shear history, as if the shear rate was a state variable of the aggregating system.

2. MODEL AND SIMULATION METHODS

We have performed simulations using a three-dimensional (3D) Brownian dynamics model in the presence of a steady shear flow. This involved solving the Langevin equation

$$m\ddot{r}_i = -\nabla U_i - \Gamma \dot{r}_i + W_i(t) + \Gamma\dot{\gamma}\left(y_i - \frac{L}{2}\right)\hat{z} \quad (1)$$

where U_i is the pair particle interaction, Γ is the drag coefficient, $W_i(t)$ is the random force acting on a particle, $\dot{\gamma}$ is the shear rate, y_i is the y component of the position vector of the ith particle, $\hat{z}$ is the unit vector along the z axis, and L is the box length. Hydrodynamic interactions, including lubrication forces, are ignored in the simulation.[19] We note that an equivalent Smoluchowski equation or a "Liouville equation on the diffusive time scale" can be written for the probability density function of the position coordinates of the Brownian particles in the system.[20]

The interparticle potential considered here is a short-range attractive potential. As a prototype, we consider the well-studied Asakura–Oosawa (AO)[21] short-range depletion potential. In particular, the potential U acting upon each colloidal particle has a 2-fold contribution: the two-body depletion potential U_{AO} plus a repulsive hard-core-like interaction U_{hc} given by the following expressions:

$$U(r_{ij}) = U_{AO}(r_{ij}) + U_{hc}(r_{ij}) \quad (2)$$

where

$$\frac{U_{AO}}{kT} = \phi_p\left(\frac{1+\zeta}{\zeta}\right)^3\left[\frac{3r_{ij}}{2(1+\zeta)} - \frac{1}{2}\left(\frac{r_{ij}}{1+\zeta}\right)^3 - 1\right] \quad \text{for } r_{ij} < 1+\zeta \quad (3a)$$

$$= 0 \quad \text{for } r_{ij} > 1+\zeta \quad (3b)$$

and

$$\frac{U_{hc}}{kT} = r_{ij}^{-\alpha} \quad (4)$$

In eq 6, ζ is the size ratio between a polymer coil and a colloidal particle, which controls the range of the depletion interaction in the AO model and ϕ_p is a parameter that controls the strength of the interaction. All of our simulations are for $\zeta = 0.1$.

In the hardcore-like repulsive interaction given by eq 4, we have set $\alpha = 36$. Exponents $\alpha < 36$ are reported to lead to anomalies when a hardcore mimic is required in the potential.[22] The total pair potential $U = U_{AO} + U_{hc}$ passes through a minimum value (U_{min}) that depends upon ζ and ϕ_p. In what follows, we will often characterize the strength of the potential in terms of the absolute value of the minimum potential depth, $U_m = |U_{min}|$, which is 10 kT in our simulations.

Our simulations used a set of reduced units, where $m = 1$, monomer diameter $\sigma = 1$, and $kT = 1$. We choose $\Gamma = 0.5$, shear rates between $\dot{\gamma} = 0.1$ and 1.0, and time step $\Delta t = 0.0001-0.005$ in reduced time units of $\sigma(m/kT)^{1/2}$. For this choice of Γ, particle motion in the absence of shear is purely diffusive for $t \gg 1/\Gamma$; i.e., $t \gg 2$ in our units. In one unit of this reduced time, a "free" monomer would diffuse a distance of $12^{1/2}\sigma$ for the value of Γ used here. A total of 40 000 monomers were randomly placed in a box of length $L = 128$ to yield a monomer volume fraction of $f_v = 0.01$. For the deep quench considered here ($U_m = 10$ kT) and in the absence of any shear, the system shows DLCA behavior similar to an irreversible, aggregating system.[23] Lees–Edwards boundary conditions were used, which is standard for shear simulations.[24] The system was allowed to develop without shear until a shear start time t_s, and then shear was turned on. Three shear start times were used: $t_s = 0$, 250, and 500. For each shear rate and shear start time, the system was allowed to reach a steady state at long times. This was monitored by the aggregation kinetics and the shape and structure of the aggregates themselves.

3. RESULTS

Figure 1a shows the average aggregate size in terms of the number of monomers per aggregate N versus time since the onset of shear. There is a zero shear rate curve, and then at three different start times (0, 250, and 500), a shear of 0.1 is turned on. This figure shows two important facts: (1) The shear enhanced the aggregation, and (2) the long-time state of the system is independent of the shear history. Figure 1b is similar to Figure 1a; only now the shear rate is 1.0. Figure 1b shows three important facts: (1) Precipitous fragmentation occurred after the shear was turned on; (2) after an induction period, in which numerous runs were shown to be stochastic,

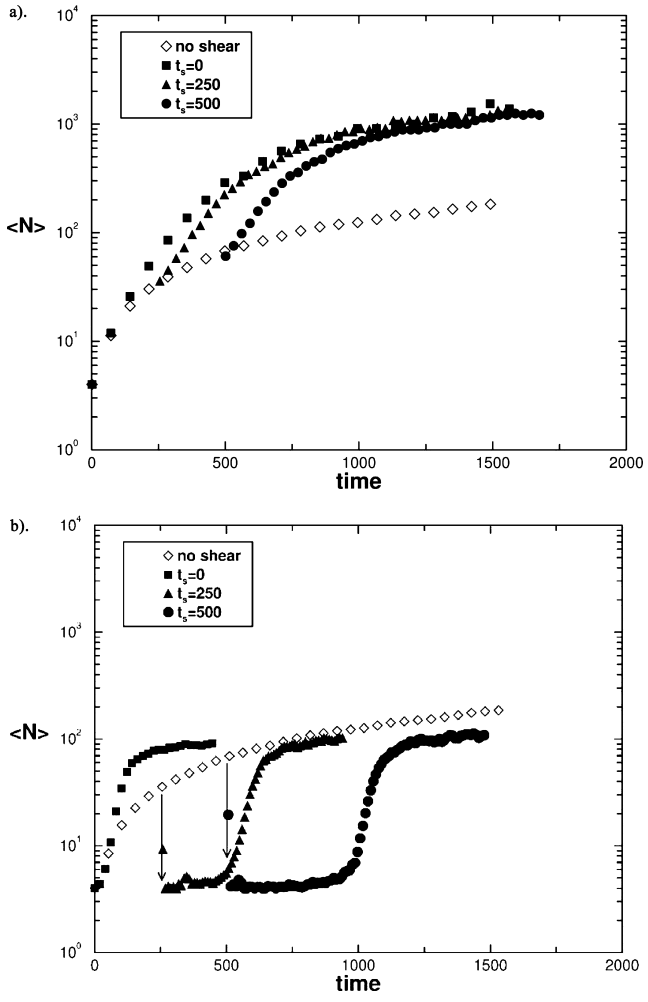

Figure 1. Average number of monomers per aggregate versus rescaled time with shear of (a) $\dot{\gamma} = 0.1$ and (b) $\dot{\gamma} = 1.0$ turned on at $t_s = 0$, 250, and 500.

dx.doi.org/10.1021/la302010e | Langmuir 2012, 28, 11337–11342

the aggregation quickly rebounds in a manner similar to classical nucleation phenomena to a regrowth period; and (3) after this regrowth, the long-time state of the system is, once again, independent of the shear history!

Other shear rates show these general features as well but with different degrees of intensity. Figure 2 shows results for a range

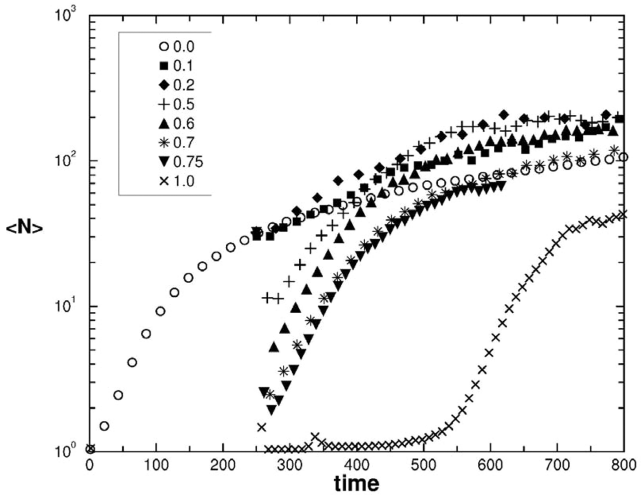

Figure 2. Average number of monomers per aggregate versus rescaled time for a variety of shear rates all turned on at t_s = 250.

of shears between 0 and 1.0, all with a start time of 250. As shear starts, the aggregates fragment to a minimum monomer number (mass). This minimum mass decreases systematically with shear and reaches total system breakdown with a shear rate of 1.0. We also note that the average aggregate mass at the steady state seems to scale with shear rate, highlighting the interplay between fragmentation and enhanced aggregation.

The structure of the aggregates can be discerned via direct real space visualization, analysis of bond-orientational order parameters, and Fourier transformation to yield the structure factor. The latter has the advantage of yielding an ensemble average and is realizable experimentally with light scattering. Zero shear yields a hybrid structure, which we have termed "fat fractals";[25,26] the monomers form dense clumps over short length scales, and then these clumps form open aggregate structure with the classic DLCA fractal dimension of D_f = 1.8. Sheared systems continue to yield fat fractals but with denser aggregates, as identified by larger fractal dimensions. A shear of 0.1 yields fractal dimensions of 2.6, as shown in Figure 3a, and a strong shear of 1.0 yields compact objects, as indicated by a Porod q^{-4} functionality for the structure factor shown in Figure 3b. However, we have not addressed large-scale anisotropy in the cluster scale in this work.

To further analyze the details of the aggregate morphology and to differentiate between the liquid- and solid-like particles in the aggregates, we use the scalar product definition of the bond orientational order parameter q_6 for the ith particle with the neighboring j particles.[27] First, we define the connected neighbors. Two neighbors are considered to be connected if the above scalar product is greater than some threshold value (chosen to be 0.65 as used in the literature[28]). For a distinction between solid- and liquid-like particles, one can set another threshold value for the number of connections. Following ref 28, any particle that has more than seven connections is considered solid-like; particles with less than or equal to seven

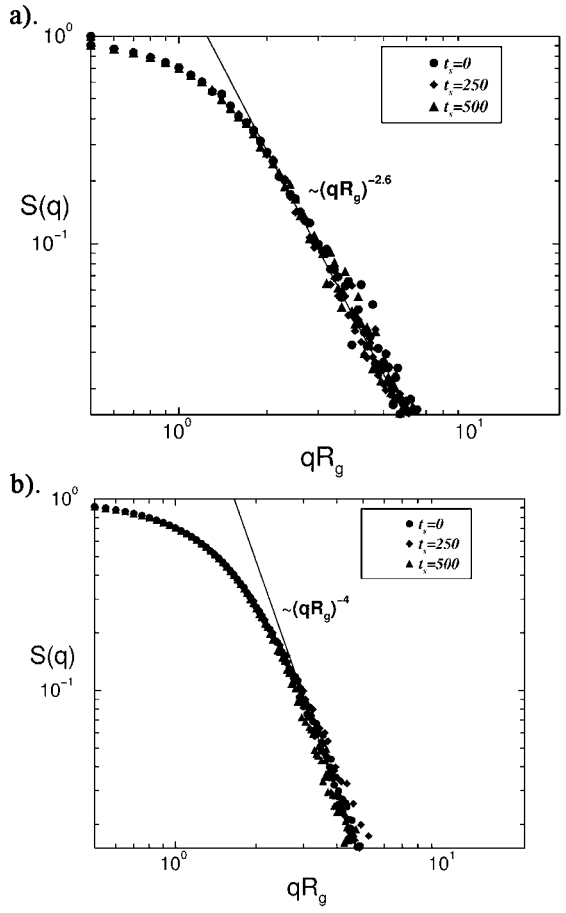

Figure 3. Structure factor for shear rate (a) $\dot{\gamma}$ = 0.1 and (b) $\dot{\gamma}$ = 1.0 with three different t_s values. In panel a, the guide line has a slope of −2.6. In panel b, aggregates are compact, indicated by the Porod q^{-4} functionality.

connections are considered as liquid-like. Once the solid- or liquid-like behavior of the particles is determined, we further assign the crystalline identity to each solid-like particle i. Figure 4 shows examples of aggregates and their crystalline structure. We observe that typical "fat fractal" aggregates in the absence of any shear is mostly liquid-like. However, aggregates corresponding to a weak shear rate of $\dot{\gamma}$ = 0.1 are more compact than the fat fractal aggregate and show large pockets of crystalline order. For a much larger shear rate of $\dot{\gamma}$ = 1.0, the aggregates are very compact and ordered but much smaller in size because of fragmentation.

It is very important to see if these fascinating numerical simulation results have anything to do with real systems. The "Rosetta Stone" to allow us to connect between the simulation and real world is the Péclet number. The Péclet number Pe is a dimensionless number that is the product of the time that it takes a particle to diffuse one diameter and the shear rate. It is a measure of the relative importance of the contributions of fluid shear and Brownian motion to the collision frequency of disperse phase clusters and monomers. Whether those collisions result in aggregation (or even breakage) events depends upon many other factors, such as the strength of the particle attractive forces and the morphology of the colliding aggregates. Generally speaking, when Pe > 1, shear is dominant, and when Pe < 1, diffusion is dominant. The dimensionless nature of Pe provides a very useful link between experimental

dx.doi.org/10.1021/la302010e | Langmuir 2012, 28, 11337−11342

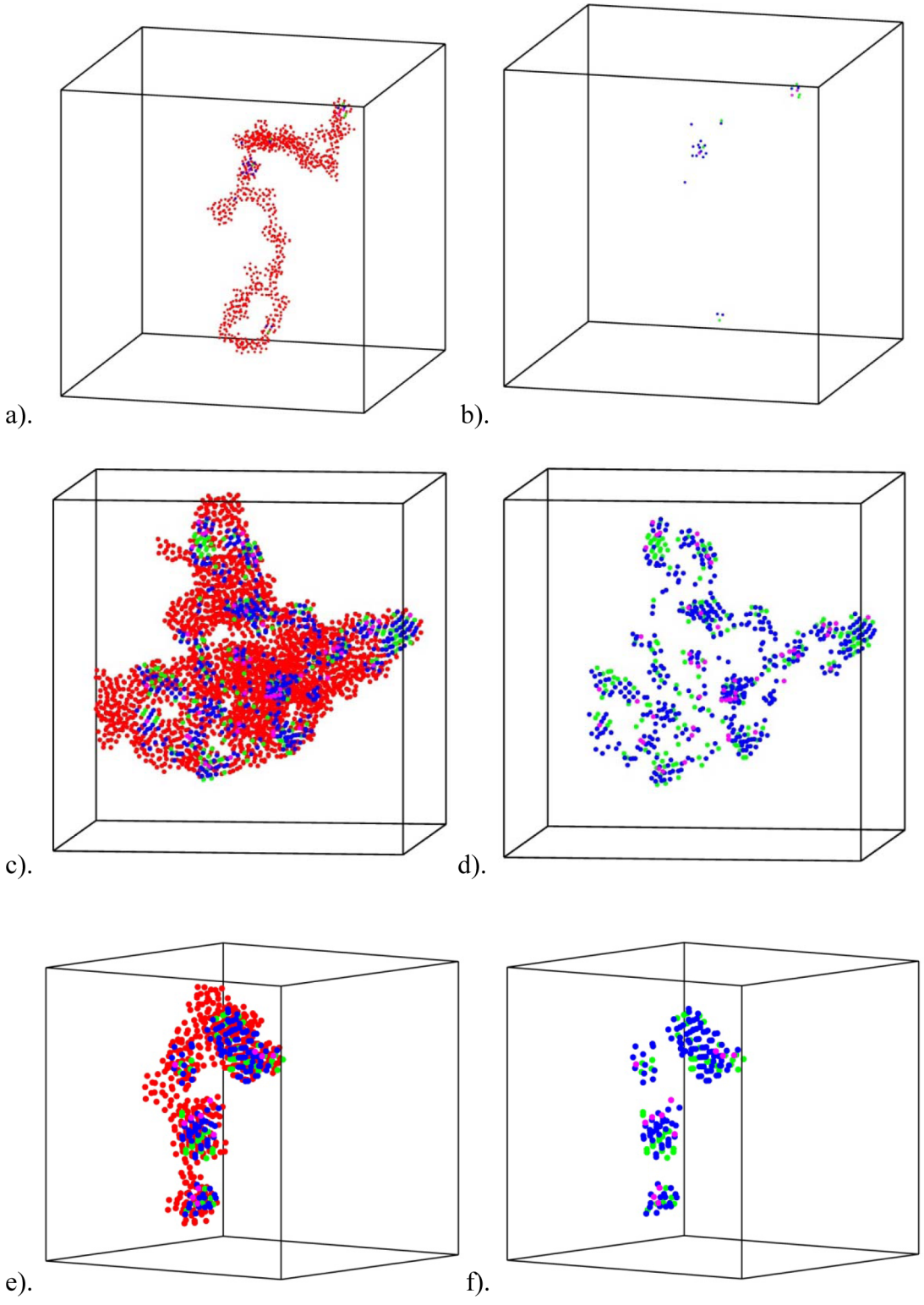

Figure 4. Red particles are liquid-like; green have face-centered cubic (fcc) structure; blue particles have hexagonal close-packed (hcp) structure; and pink particles have some other ordering. (a) Typical "fat fractal" aggregate when no shear is applied. (b) Only the crystalline particles of the aggregate shown in panel a are shown. (c) Aggregate formed under a shear rate of $\dot{\gamma} = 0.1$. Note that the aggregate is more compact than the fat fractal aggregate and also shows large pockets of crystalline order. (d) Only the crystalline particles of the aggregate shown in panel c are shown. (e) Aggregate formed under a shear rate of $\dot{\gamma} = 1.0$. Now the aggregate has pockets of crystalline order, but it is smaller in size than $\dot{\gamma} = 0.1$ aggregates because of fragmentation. (f) Only the crystalline parts of the aggregate shown in panel e are shown.

and numerical simulations. The Péclet number is commonly written as

$$Pe = \frac{6\pi\eta R_m{}^3\dot{\gamma}}{kT} \quad (5)$$

dx.doi.org/10.1021/la302010e | *Langmuir* 2012, 28, 11337−11342

where η is the viscosity, R_m is the particle mobility radius, and $\dot{\gamma}$ is the shear rate. The drag coefficient Γ is related to the viscosity by $\Gamma = 6\pi\eta R_m$. Thus, the Péclet number becomes

$$Pe = \frac{\Gamma {R_m}^2}{kT}\dot{\gamma} \quad (6)$$

.In our simulation, $\Gamma = 0.5$, $kT = 1$, and $\dot{\gamma} = 0.1-1$. When shear is turned on from the beginning, we use $R_m = 0.5$ to yield $Pe = 0.0125-0.125$. In the other extreme, for start times of 500, R_m begins around 2.3 to yield $Pe = 0.26-2.6$. These Péclet numbers are well in the range accessible to experiments to imply that the remarkable results seen in the simulation should appear in real world experiments as well. For example, the Péclet numbers for the experimental studies cited in the Introduction[17,18] range from 0.01 to 260.

4. SUMMARY AND CONCLUSIONS

In summary, numerical simulations of aggregation in the presence of shear in a model colloidal system characterized by short-range attractive potential shows that weak shear enhances the aggregation process, while strong shear leads to fragmentation and subsequent nucleation and rebound in cluster growth after an induction time. A detailed energetic and entropic theory of aggregation that can explain these phenomena is lacking at present. However, a few general comments can be made. To restructure or break up flocs under shear flow, local stresses must create forces on a pair of particles stronger than the interparticle attraction. For relatively mild shears, apparently clusters can simply undergo rearrangement into structures with sufficient strength to prevent breakage. Above some threshold of shear, fat fractal aggregates are simply too fragile to survive and, consequently, are destroyed and eventually replaced by compact, pseudo-crystalline aggregates. We should further note that Brownian dynamics ignores the effect of the particles on the flow, producing a "free-draining" floc. That produces stronger stresses within the flow and weaker stresses on the periphery, which should have implications on the breakup. What is striking though is that, in each case, the long-time state of the system is independent of the shear history, to imply that the shear rate acts as a state variable of the aggregating system. We expect our results to be valid for general short-range attractive potentials with a deep well depth. Further studies are needed to elucidate how the depth and range of this attractive potential affect the shear-induced aggregation and breakup.

AUTHOR INFORMATION

Corresponding Author

*E-mail: amitc@phys.ksu.edu.

Notes

The authors declare no competing financial interest.

ACKNOWLEDGMENTS

This work was supported by a Targeted Excellence award from the Kansas State University. We thank Siddique J. Khan for considerable help with the numerical simulations.

REFERENCES

(1) Goodwin, J. *Colloids and Interfaces with Surfactants and Polymers*; Wiley: New York, 2004.

(2) Serra, T.; Colomer, J.; Casamitjana, X. Aggregation and breakup of particles in a shear flow. *J. Colloid Interface Sci.* **1997**, *187*, 466−473.

(3) Torres, F. E.; Russel, W. B.; Schowalter, W. R. Floc structure and growth kinetics for rapid shear coagulation of polystyrene colloids. *J. Colloid Interface Sci.* **1991**, *142*, 554−574.

(4) Serra, T.; Casamitjana, X. Structure of the aggregates during the process of aggregation and breakup under a shear flow. *J. Colloid Interface Sci.* **1998**, *206*, 505−511.

(5) Kikuchi, Y.; Yamada, H.; Kunimori, H.; Tsukada, T.; Hozawa, M.; Yokoyama, C.; Kubo, M. Aggregation behavior of latex particles in shear flow confined between two parallel plates. *Langmuir* **2005**, *21*, 3273−3278.

(6) Selomulya, C.; Bushell, G.; Amal, R.; Waite, T. D. Aggregation mechanisms of latex of different particle sizes in a controlled shear environment. *Langmuir* **2002**, *18*, 1974−1984.

(7) Lin, M. Y.; Klein, R.; Lindsay, H. M.; Weitz, D. A.; Ball, R. C.; Meakin, P. The structure of fractal colloidal aggregates of finite extent. *J. Colloid Interface Sci.* **1990**, *137*, 263−280.

(8) Lindsay, H. M; Lin, M. Y.; Weitz, D. A.; Sheng, P.; Chen, Z.; Klein, R.; Meakin, P. Properties of fractal colloid aggregates. *Faraday Discuss. Chem. Soc.* **1987**, *83*, 153−165.

(9) Martin, J. E.; Wilcoxon, J. P.; Schaefer, D.; Odinek, J. Fast aggregation of colloidal silica. *Phys. Rev. A: At., Mol., Opt. Phys.* **1990**, *41*, 4379−4391.

(10) Jung, S. J.; Amal, R.; Raper, J. A. Monitoring effects of shearing on floc structure using small-angle light scattering. *Powder Technol.* **1996**, *88*, 51−54.

(11) Wang, L.; Marchisio, D. L.; Vigil, R. D.; Fox, R. O. CFD simulation of aggregation and breakage processes in laminar Taylor−Couette flow. *J. Colloid Interface Sci.* **2005**, *282*, 380−396.

(12) Oles, V. Shear-induced aggregation and breakup of polystyrene latex particles. *J. Colloid Interface Sci.* **1992**, *154*, 351−358.

(13) Vanni, M.; Gastaldi, A. Hydrodynamic forces and critical stresses in low-density aggregates under shear flow. *Langmuir* **2011**, *27*, 12822−12833.

(14) Frappier, G.; Lartiges, B. S.; Skali-Lami, S. Floc cohesive force in reversible aggregation: A Couette laminar flow investigation. *Langmuir* **2010**, *26* (13), 10475−10488.

(15) Becker, V.; Briesen, H. A master curve for the onset of shear induced restructuring of fractal colloidal aggregates. *J. Colloid Interface Sci.* **2010**, *346*, 32−36.

(16) Zaccone, A.; Soos, M.; Lattuada, M.; Wu, H.; Bäbler, M. U.; Morbidelli, M. Breakup of dense colloidal aggregates under hydrodynamic stresses. *Phys. Rev. E: Stat. Phys., Plasmas, Fluids, Relat. Interdiscip. Top.* **2009**, *79*, 061401.

(17) Huang, H.; Sorensen, C. M. Shear effects during the gelation of aqueous gelatin. *Phys. Rev. E: Stat. Phys., Plasmas, Fluids, Relat. Interdiscip. Top.* **1996**, *53*, 5075.

(18) Mokhtari, T.; Chakrabarti, A.; Sorensen, C. M.; Cheng, C.-Y.; Vigil, D. The effect of shear on colloidal aggregation and gelation using small angle light scattering. *J. Colloid Interface Sci.* **2008**, *327*, 216−223.

(19) Riese, D. O.; Wegdam, G. H.; Vos, W. L.; Sprik, R.; Fenistein, D.; Bongaerts, J. H. H.; Grübel, G. Effective screening of hydrodynamic interactions in charged colloidal suspensions. *Phys. Rev. Lett.* **2000**, *85*, 6460−5463.

(20) Dhont, J. K. G. Shear induced displacement of the spinodal of Brownian systems. *Phys. Rev. Lett.* **1996**, *76*, 4269−4272.

(21) Asakura, S.; Oosawa, F. Interaction between particles suspended in solutions of macromolecules. *J. Chem. Phys.* **1954**, *22*, 1255.

(22) Melrose, J. R. Aggregate networks under shear. *Europhys. Lett.* **1992**, *19*, 51.

(23) Khan, S. J.; Sorensen, C. M.; Chakrabarti, A. Kinetics and morphology of cluster growth in a model of short-range attractive colloids. *J. Chem. Phys.* **2009**, *131*, 194908.

(24) Lees, A. W.; Edwards, S. F. The computer study of transport processes under extreme conditions. *J. Phys. C.* **1972**, *5*, 1921.

(25) Chakrabarti, A.; Fry, D.; Sorensen, C. M. Molecular dynamics simulation of the transition from dispersed to solid phase. *Phys. Rev. E: Stat. Phys., Plasmas, Fluids, Relat. Interdiscip. Top.* **2004**, *69*, 031408.

(26) Skjeltorp, A. T. Visualization and characterization of colloidal growth from ramified to faceted structures. *Phys. Rev. Lett.* **1987**, *58*, 1444−1447.
(27) ten Wolde, P. R.; Ruiz-Montero, M. J.; Frenkel, D. Numerical calculation of the rate of crystal nucleation in a Lennard−Jones system at moderate undercooling. *J. Chem. Phys.* **1996**, *104*, 9932−9947.
(28) ten Wolde, P. R.; Ruiz-Montero, M. J.; Frenkel, D. Simulation of homogeneous crystal nucleation close to coexistence. *Faraday Discuss.* **1996**, *104*, 93−110.